IJCRT.ORG ISSN : 2320-2882

INTERNATIONAL JOURNAL OF CREATIVE RESEARCH THOUGHTS (IJCRT)

An International Open Access, Peer-reviewed, Refereed Journal

Power Factor Correction in SRM Motor Drives Using Boost Converter in Continuous Conduction Mode

A.V. Somadhitya1, Dr. V. Srinivasa Rao2, K. Rambabu3
P.G. Scholar1, Professor2, Associate Professor3
Department of Electrical and Electronics Engineering,
1Aditya Engineering College (A), Surampalem, Andhra Pradesh, India

Abstract: The typical modelling for dc–dc converters, which is commonly extended to rectifiers, provides a more accurate analysis. Several PFC approaches developed from transfer functions may be quickly and concisely implemented using this methodology. It is shown how to construct a boost-based PFC stage in a switching reluctance motor (SRM) utilizing the well-known one-cycle controls technique (OCC) at AC mains. SRM is an excellent choice for low-power domestic applications because to its simple structure and winding-free rotor. By adjusting the DC-bus voltage across the proposed converter of SRM, SRM may be sped up or slow down. Power quality at the AC mains is improved by using a suggested converter that operates in discontinuous inductor current mode. MATLAB Simulation Simulink software is used to display the simulation results.

Index Terms **- Switched Reluctance Motor (SRM), one-cycle control technique (OCC).**

I. INTRODUCTION

Electrical drives are a vital part of many commercial and industrial processes. Permanent magnet brushless motors have been replaced with switchable reluctance motors in many industrial applications. Switched reluctance motors have a large torque ripple, a high acoustic ripple, and are difficult to manage because of this. Because of the rise in the power of electronic gadgets, the switched reluctance motor has gotten more attention. In terms of mechanical and electrical roughness, switched reluctance motors are more abrasive than typical AC and DC motors. Non-linear torque pulsation is caused by the SRM's discrete torque mechanism. The purpose of an air conditioner is to keep the temperature of the surrounding air at a constant level. Only by adjusting the speed of the compressor's drive can the air conditioning system's compressor attain a higher level of efficiency. With a switching reluctance motor, an air conditioning system may be built cheaply and last a long time. A motor's rotational speed may be adjusted by adjusting the D.C link voltage, which is inversely proportional to the motor's revolutions per minute.

Based on the SRM's rotor position sensor and hysteresis current control technology, the switch of the asymmetric bridge converter is activated or deactivated. A large peak in ac input current is caused by an essentially uncontrolled charging of the D.C link capacitor. A low power factor (PF), high total harmonic distortion (THD), and a high crest factor are all symptoms of an out-of-control capacitor charging (CF). In this study, a Cuk D.C-D.C converter is presented as a voltage control drive. A PFC converter with a broad range of output voltage and a tiny output capacitive and inductive filter is required for voltage-controlled drive applications. All of the specifications for the PFC converter are met by the Cuk converter. D.C. link voltage regulation may also be achieved by using the proposed architecture.

II. PFC BOOST CONVERTER IN CCM

Because single-stage converters may offer near unity power factor, control of output voltage, minimal device count and decreased low-frequency ripple in general, they are the simplest approach for implementing a general-purpose switched-mode power supply SMPS [21]. As an added benefit, depending on the application, a high-voltage dc connection may be used, reducing the low-frequency filtering capacitance to the point where long-life film capacitors may be used.

There are a few hundred-watt PFC applications where a single-stage AC–DC boost converter is the most common choice because to its inherent simplicity, decreased number of power stage parts, and constant input current. In addition, it reduces the strains on the semiconductors, those are directly proportional to the input current. With the ac–dc boost setup as shown in Fig. 1, many control methods may be used to create PFC. As a popular solution due to the availability of commercially available ICs, ACMC has increased complexity and a greater component count in the control system. Since they don't need multipliers, divisions, or a sample of the

rectified input voltage [8], indirect approaches like the OCC may overcome these disadvantages. According to the sections [22–24] of this paper, IR1150 is the sole commercial IC specialized to OCC.

Equations (1) and (2) provide the equations for computing the ac- dc boost converter's filter elements, i.e. Lm and Cd.

$$L_m = \frac{V_g}{f_s(PFC)} \cdot \frac{\Delta I_{Lb}}{\Delta \mathrm{I_{Lb}}} \quad (1)$$

$$C_d = \frac{P_1}{2\cdot(2\pi f_L)\cdot V_{dc}\cdot\Delta V_{dc}} \quad (2)$$

$$\beta = \frac{V_{dc}}{V_g} \quad (3)$$

$$\Delta I_{Lm} = \frac{\beta}{4} \quad (4)$$

Peak input voltage, switching frequency (fs(PFC)), standardised inductor current ripple (ILm) set forth by a variable, inductor current ripple at high grid voltage, rated output power (Po), line frequency (fL), average dc-link voltage (Vdc), and ripple in dc-link voltage (Vdc).

A new segment on the evolution of an easier PFC small-signal modelling technique will focus on the ac-dc boost converter. This method consider for account the ac mains' small-frequency dynamics and the requirement for substantial dc-link capacitances in the execution of various control approaches.

III. PROPOSED CONCEPT

When using PFC converters in CCM, the dc-link voltage is dominated by a low-frequency component that has a direct impact on system dynamics. As a result, an average analysis of the ac grid voltage during a half period provides a better representation of the modeling methods. Active switches and diodes are replaced by controlled current sources to create small-signal disruptions in the average current flowing through semiconductors in this technique. Afterwards, this model may be used to examine the impact of interruption on the PFC converter.

The first step is to establish the settings of a PFC boost converter in CCM. Figure 2 shows some common low- and high-frequency waveforms, from which several useful formulas may be derived. Reconciled sinusoidal input voltage and duty cycle are obtained by Equations (5) and (6), which are both time-variant.

$$v_g(t) = V_g \cdot |\sin(\omega_L t)| \quad (5)$$

$$\frac{V_{dc}}{V_g\cdot\sin(\omega_L t)} = \frac{1}{1-d(t)} \Rightarrow d(t) = 1 - \frac{V_g\cdot\sin(\omega_L t)}{V_{dc}} \quad (6)$$

The analysis is made simpler by assuming that the inductor current will remain constant during the switching time Ts. Therefore, by just taking into account the positive half-cycle of the grid voltage, it is possible to express the average value of the instantaneous inductor current as a rectified sinusoidal waveform.

Equation then describes the average values of the instantaneous input voltage and inductor current (7).

$$\langle i_{Lm}\rangle_{Ts} = I_{Lm}\cdot\sin(\theta), 0 < \theta < \pi$$

$$\langle v_g\rangle_{Ts} = v_g\cdot\sin(\theta), 0 < \theta < \pi \quad (7)$$

Here Lt is the phase angle in rad and ILm is the peak current through the filter inductor's instantaneous average value.

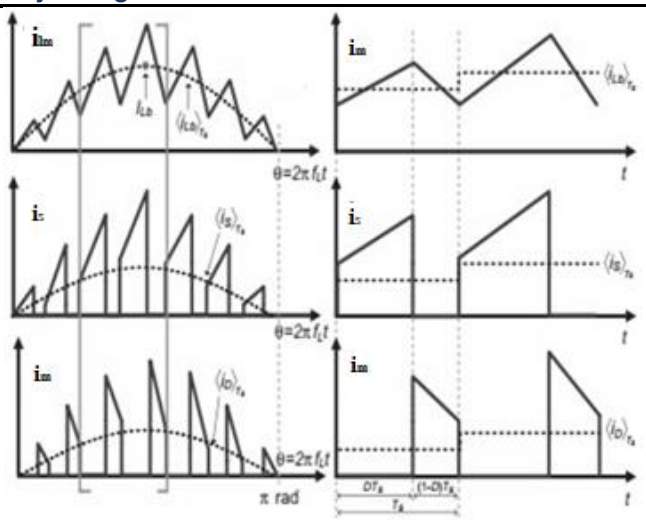

Figure 1 shows an in-depth view a PFC boost rectifier's typical low- and high-frequency waveforms in CCM. In this figure, vg(t) denotes the immediate input voltage, L=2fL denotes the line angular frequency in rad/s, and d(t) denotes the time-variant duty cycle. According to the high-frequency wave patterns in Figure 2, the currents via the active switch and diode must also be characterised by their corresponding average values throughout one switching period, leading to gin:

$$\langle i_s \rangle_{Ts} = d(t) \cdot \langle i_{Lm} \rangle_{Ts}$$

$$\langle i_{Di} \rangle_{Ts} = \big(1 - d(t)\big) \cdot \langle i_{Lm} \rangle_{Ts} \qquad (8)$$

Equation (9) can be produced by substituting the duty cycle and inductor current given by Equations (6) and (7), respectively, in Equation (8).

$$\langle i_s \rangle_{Ts}(t) = \left(1 - \frac{V_g \sin(\theta)}{V_{dc}}\right) \cdot (I_{Lm} \cdot \sin(\theta))$$

$$\langle i_{Di} \rangle_{Ts}\ (t) = \left(\frac{V_g \sin(\theta)}{V_{dc}}\right) \cdot (I_{Lm} \cdot \sin(\theta)) \qquad (9)$$

For example, TL/2 = 1/(2fL) = It is necessary to integrate the average current while taking into account one period of the rectified input voltage for the active switch and diode specified in Equations (10) and (11), respectively. Since the currents can be expressed in terms of both high- and low-frequency components, they are characterised in Equations (10) and (11).

$I_S = \langle \langle i_s \rangle_{Ts} \rangle T_{L/2} = \frac{1}{\pi} \cdot \int_0^{\pi} \langle i_s \rangle_{Ts}(\theta) d\theta$

- $I_S = \frac{1}{\pi} \cdot \int_0^{\pi} \left[I_{Lm} \cdot |\sin(\theta)| - \frac{I_{Lb} \cdot v_g}{V_{dc}} (|\sin\theta|)^2 \right] d\theta$
- $I_S = I_{Lm} \cdot \left(\frac{2}{\pi} - \frac{V_g}{2 \cdot V_{dc}}\right)$ (10)

$$I_D = \langle \langle i_z \rangle_{Ts} \rangle T_{L/2} = \frac{1}{\pi} \cdot \int_0^{\pi} \langle i_D \rangle_{Ts}(\theta) d\theta$$

$$I_{Di} = \frac{1}{\pi} \cdot \int_0^{\pi} \left[\frac{I_{Lb} \cdot V_g}{V_{dc}} (|\sin\theta|)^2 \right] d\theta$$

$$I_{Di} = \frac{I_{Lb} \cdot V_g}{2 \cdot V_{dc}} \qquad (11)$$

On the basis of perturbing and linearizing average circuit variables, the average The frequency domain can be used to express small-signal models. For the average currents to be represented in Laplace, each input parameter must be perturbed. The disturbance is provided by Equation (1) when the active switch is taken into account (12).

$$\Delta\langle\langle i_s\rangle_{Ts}\rangle T_{L/2} = G_{sg} v_g + G_{So} \cdot v_{dc} + G_{si} \cdot i_{Lb} \quad (12)$$

Here, GSg, GSo and GSi are the partial derivatives of the active switch current, respectively, with regard to the inductor current, input voltage and output voltage. The disturbances related with the input voltage, dc-link voltage and inductor current are also included in the equations. Using Equation 1, we may express the time-dependent expression in the frequency domain (13).

$$i_S(s) = G_{sg} \cdot V_g(s) + G_{So} \cdot V_{dc}(s) + G_{si} \cdot i_{Lb}(s) \quad (13)$$

where v g(s), vdc(s), and iLb(s) are the frequency-domain representations of the input voltage, output voltage, and inductor current. The linearized operating point must be taken into account while solving the partial derivatives of the switch current. Thus, Equations (14)–(16) are the consequence of substituting Equation (12) in Equation (12). (10).

$$G_{sg} = \frac{\partial}{\partial V_g}\left[I_{Lm}\left(\frac{2}{\pi} - \frac{V_g}{2V_{dc}}\right)\right] = -\frac{I_{Lm}}{2V_{dc}} \quad (14)$$

$$G_{So} = \frac{\partial}{\partial V_{dc}}\left[I_{Lm}\left(\frac{2}{\pi} - \frac{V_g}{2V_{dc}}\right)\right] = \frac{I_{Lm} \cdot V_g}{2{V_{dc}}^2} \quad (15)$$

$$G_{Si} = \frac{\partial}{\partial I_{Lm}}\left[I_{Lb}\left(\frac{2}{\pi} - \frac{V_g}{2V_{dc}}\right)\right] = \frac{2}{\pi} - \frac{V_g}{2V_{dc}} \quad (16)$$

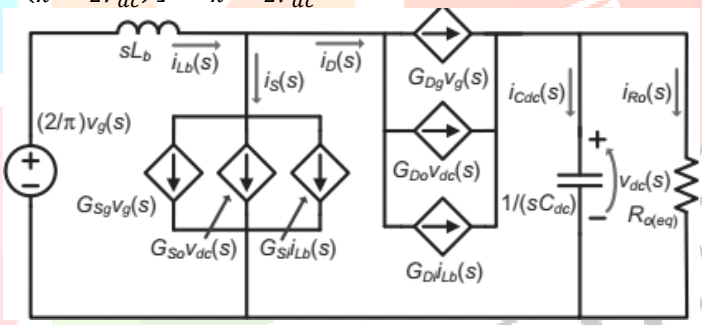

Figure 2 The PFC boost rectifier's average equivalent circuit in CCM

Equation (17) states that the identical analysis carried out in the frequency domain for the passive switch, or diode (18)

$$\Delta\langle\langle i_{Di}\rangle_{Ts}\rangle T_{L/2} = G_{Dg} v_g + G_{Do} \cdot v_{dc} + G_{Di} \cdot i_{Lm} \quad (17)$$

Where the partial derivatives of the diode current with relation input voltage, output voltage, and inductor current, respectively, are denoted by the letters GDg, GDo, and GDi.

$$i_{Di}(s) = G_{Dg} \cdot V_g(s) + G_{Do} \cdot V_{dc}(s) + G_{Di} \cdot i_{Lb}(s) \quad (18)$$

$$G_{Dg} = \frac{\partial}{\partial V_g}\left[\frac{I_{Lb} \cdot V_g}{2V_{dc}}\right] = \frac{I_{Lb}}{2V_{dc}} \quad (19)$$

$$G_{Do} = \frac{\partial}{\partial V_{dc}}\left[\frac{I_{Lb} \cdot V_g}{2V_{dc}}\right] = -\frac{I_{Lb} \cdot V_g}{2{V_{dc}}^2} \quad (20)$$

$$G_{Di} = \frac{\partial}{\partial V_{Lb}}\left[\frac{I_{Lb} \cdot V_g}{2V_{dc}}\right] = \frac{V_g}{2V_{dc}} \quad (21)$$

The high inductor current ILb is calculable using the power balance that is applied to this element as indicated by Equation (22).

$$\frac{I_{Lb} \cdot V_g}{2} = P_o \therefore I_{Lm} = \frac{2 \cdot P_o}{V_g} \quad (22)$$

$$Z_{v(ESR)}(s) = \frac{V_{dc}(s)}{i_{Lm}(s)} = \frac{R_{o(eq)} \cdot G_{Di}}{1 - R_{o(eq)} \cdot G_{Do} + \frac{s(R_{o(eq)} \cdot C_{dc})}{s(ESR \cdot C_{dc}+1)}}$$

IV. SIMULATION RESULTS

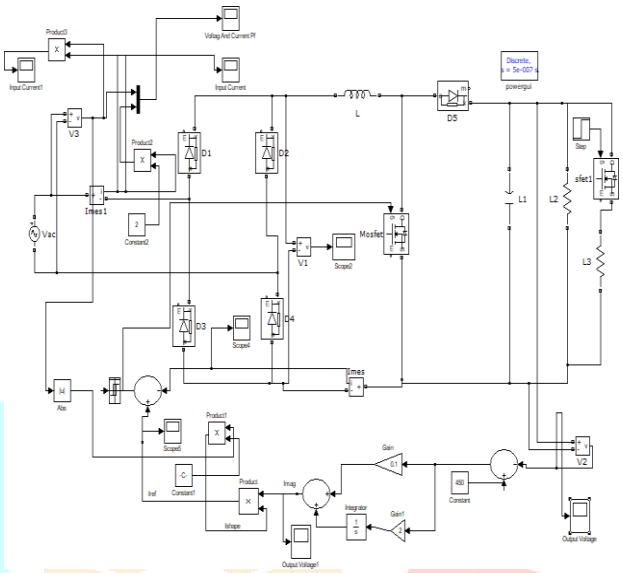

Figure 3 Simulink Diagram of Proposed DC-DC Converter with Increasing of Load

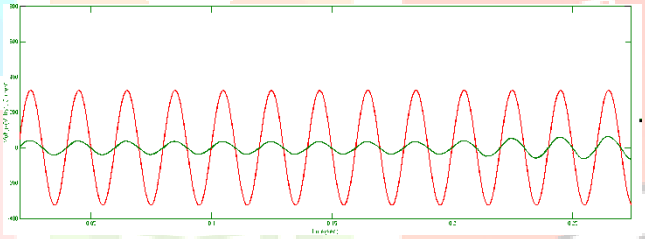

Figure 4 Simulation waveform of Proposed DC-DC Converter with Increasing of Load Input voltage & Current

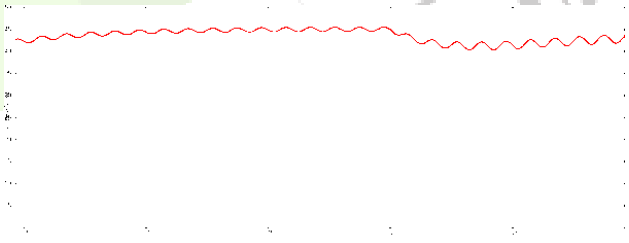

Figure5 Simulation waveform of Proposed DC-DC Converter with increasing of Load output voltage

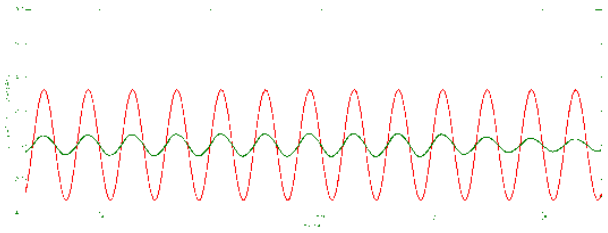

Figure 6 Simulation waveform of Proposed DC-DC Converter with Decreasing of Load Input voltage & Current

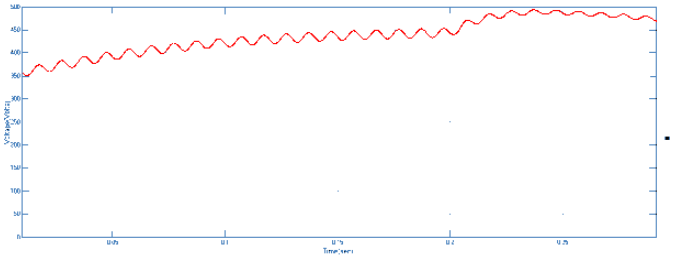

Figure 7 Simulation waveform of Proposed DC-DC Converter with Decreasing of Load output voltage & Current

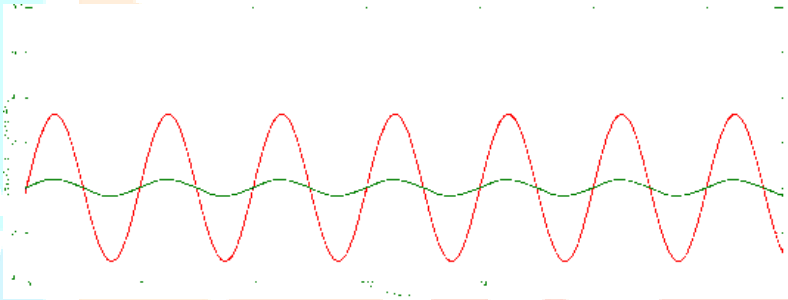

Figure 8 Simulation waveform of Proposed DC-DC Converter with Fixed of Load Input voltage & Current

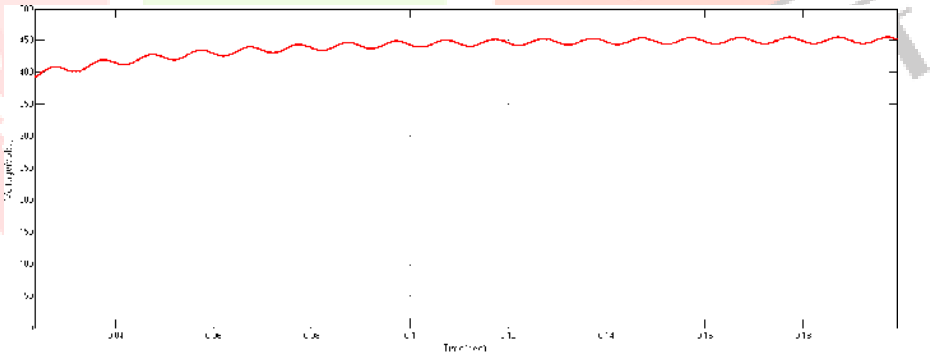

Figure 9 SimulationwaveformofProposed DC-DC Converter with Fixed of Load Ouput voltage

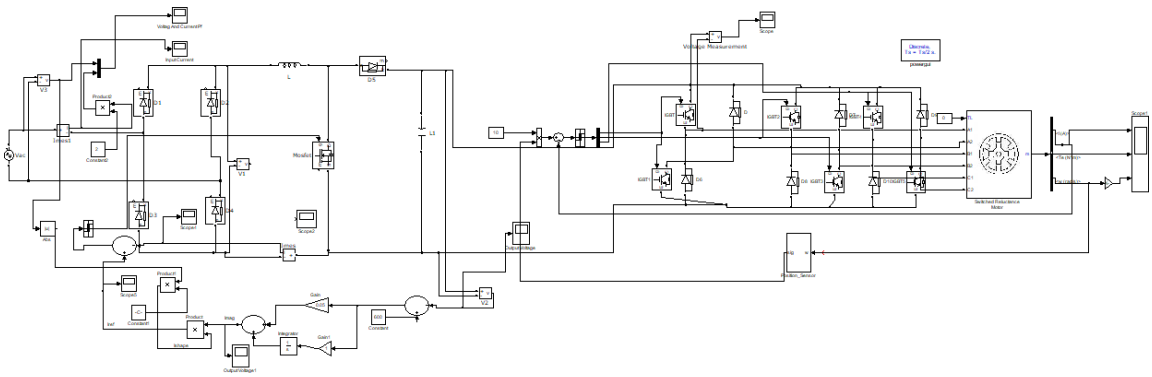

Figure 10 Simulink Diagram of Proposed DC-DC Converter with SRM Motor Drive Application

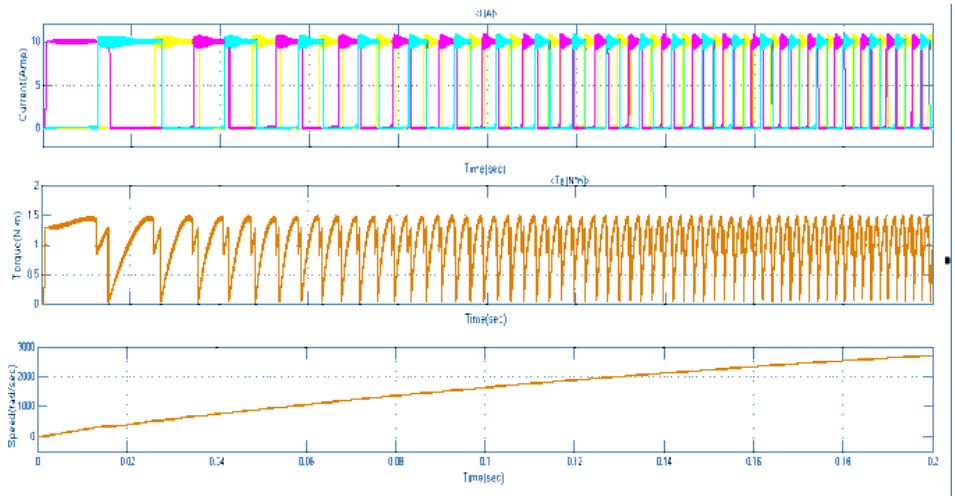

Figure11 Simulationwaveform of Proposed DC-DC Converter with SRM Motor Drive Performance of Stator current, Torque & Speed Characteristics

V. CONCLUSION

A low-power SRM driven by a switching capacitor buck boost converter has been presented. MATLAB/Simulink has been used to develop the converter and run associated simulations to evaluate performance. Small-signal modelling of PFC rectifiers functioning in CCM has been reported in this paper. When peak-value filter capacitors are used, the low-frequency dynamics of these converters cannot be accurately reproduced by conventional methods those are average state space and PWM switch models. As a result, the introduced methodology can be considered a simple, concise, and easy to understand solution. A popular architecture for general-purpose applications led to the selection of a front-end boost rectifier, which was thoroughly analyzed.

Using relevant waveforms in the time and frequency domains, the small-signal model was shown to accurately reproduce the PFC rectifier's behavior notwithstanding the fact that high-value applied. To confirm accuracy and application of the suggested low-frequency modelling approach, only minor deviations were validated using a simulated model using a closed-loop control system that evaluated overshoot and settling time.

REFERENCES

[1]. de Castro Pereira, Denis & Rosa, Bruno & Soares, Guilherme & Almeida, Pedro & Tofoli, Fernando & Braga, Henrique. (2021). Improved and accurate low-frequency average modelling and control of a conventional power factor correction boost converter in continuous conduction mode. IET Power Electronics. 14. 373-385. 10.1049/pel2.12039.

[2]. L. Roggia, J. E. Baggio and J. R. Pinheiro, "Predictive current controller for a power factor correction boost converter operating in mixed conduction mode," *2009 13th European Conference on Power Electronics and Applications*, 2009, pp. 1-10.

[3]. Qi, W., et al.: Design concerns for voltage sensor less manage of a PFC unmarried-phase rectifier without electrolytic capacitors. IEEE Trans. Indust. Electron. Sixty seven(three), 1878–1889 (2020)

[4]. Dong, H., et al.: A novel primary-side regulation manage scheme for CCM and DCM LLC LED motive force primarily based on “magnetizing modern cancellation technique. IEEE Trans. Power Electron. 35(11), 12223–12237 (2020)

[5]. M. J. Esfandani, M. Feizi and R. Beiranvand, "CCM Operation of a Single-Stage Boost-Flyback Converter with Active-Clamp for LED Driver Applications," *2020 11th Power Electronics, Drive Systems, and Technologies Conference (PEDSTC)*, 2020, pp. 1-6, doi: 10.1109/PEDSTC49159.2020.9088460.

[6]. Electromagnetic compatibility (EMC) - Part 3-4: Limits - Limitation of emission of harmonic currents in low-voltage power deliver systems for gadgetwith rated cutting-edge extra than sixteen A. IEC 61000-three-4. International Electrotechnical Commission, Geneva (2014)

[7]. Fischer, G.S., et al.: Extensions of main-edge modulated one-cycle manipulate for totem bridgeless rectifiers. IEEE Trans. Power Electron. 35(five), 5447–5460 (2020)

[8]. M. Bouaraki, F. Z. Dekhandji and A. Recioui, "Design and Simulation of Low Distortion Current Mode Control Power Factor Correction Converter," *2020 International Conference on Electrical Engineering (ICEE)*, 2020, pp. 1-6, doi: 10.1109/ICEE49691.2020.9249814.

[9]. Smedley, K.M., Cuk, S.: One-cycle manipulate of switching converters. IEEE ´ Trans. Power Electron. 10(6), 625–633 (1995)

[10]. Borgonovo, D., et al.: A self-controlled electricity thing correction singlephase improve pre-regulator In: thirty sixth Power Electronics Specialists Conference PESC’05. IEEE, Piscataway, New Jersey, pp. 2351–2357 (2005)

[11]. Middlebrook, R.D., Cuk, S.: A wellknown unified technique to modelling switching-converter energy stages. In: Power Electronics Specialists Conference. IEEE, Piscataway, New Jersey, pp. 18–34 (1976)

[12]. Cuk, S., Middlebrook, R.D.: A considerable unified method to modelling switching DC-to-DC converters in discontinuous conduction mode. In: Power Electronics Specialists Conference. IEEE, Piscataway, New Jersey, pp. 36– 57 (1977)

[13]. Polivka, W.M., et al.: State-space average modelling of converters with parasitics and storage-time modulation. In: Power Electronics Specialists Conference. IEEE, Piscataway, New Jersey, pp. 119–143 (1980)

[14]. Smithson, S.C., Williamson, S.S.: A unified state-space model of constant frequency present day mode-managed power converters in non-stop conduction mode. IEEE Trans. Indust. Electron. 62(7), 4514–4524 (2015)

[15]. Vorperian, V.: Simplified evaluation of PWM converters the usage of model of PWM transfer. Continuous conduction mode. IEEE Trans. Aerosp. Electron. Syst. 26(3), 490–496 (1990)

[16]. Vorperian, V.: Simplified evaluation of PWM converters the usage of model of PWM switch. II. Discontinuous conduction mode.IEEE Trans. Aerosp. Electron. Syst. 26(three), 497–505 (1990)

[17]. Migoni, G.A., et al.: A blended modeling approach for green simulation of PWM switching mode electricity resources. IEEE Trans. Power Electron. 34(10), 9758–9767 (2019)

[18]. Nabinejad, A., et al.: A systematic technique to extract kingdom space averaged equations and small signal model of partial energy converters. IEEE Journal of Emerging and Selected Topics in Power Electronics 8(three), 2475–2483 (2020)

[19]. Rajagopalan, J., et al.: A trendy technique for derivation of average cutting-edge mode manipulate laws for unmarried-segment energy-aspect-correction circuits with out input voltage sensing. IEEE Trans. Power Electron. 14(four), 663–672 (1999)

[20]. Choi, B., et al.: Modeling and small-sign evaluation of managed ontime boost power-element-correction circuit. IEEE Trans. Indust. Electron 48(1), 136–142 (2001)

[21]. Alonso, J.M., et al.: A honest technique to modeling excessive energy aspect ac–dc converters. IEEE Trans. Power Electron. 28(10), 4723–4731 (2013)

[22]. Fang, P., et al.: A multiplexing ripple cancellation led motive force with genuine singlestage strength conversion and flicker-free operation. IEEE Trans. Power Electron. 34(10), 10105–10120 (2019)

[23]. Brown, R., Soldano, M.: One cycle manage IC simplifies PFC designs. In: APEC 2005: Twentieth Annual IEEE Applied Power Electronics Conference and Exposition. IEEE, Austin, Texas 825–829 (2005)

[24]. Tiwari, S., et al.: Efficiency and carried out EMI assessment of a single phase electricity facto correction enhance converter the use of modern-day SiC MOSFET and SiC diode. IEEE Trans. Ind. Appl. 55(6), 7745–7756 (2019)

[25]. Bamgboje, D.O., et al.: Low fee excessive overall performance LED driving force based on a self-oscillating boost converter. IEEE Trans. Power Electron. 34(10), 10021–10034 (2019).